

6-28-2011

A Comparative Analysis of Different Fields of View in Cone Beam Computed Tomography Imaging to Identify the Inferior Alveolar Nerve Canal

Ibrahim Yamany
dr_ibrahim_yamany@yahoo.com

Recommended Citation

Yamany, Ibrahim, "A Comparative Analysis of Different Fields of View in Cone Beam Computed Tomography Imaging to Identify the Inferior Alveolar Nerve Canal" (2011). *Master's Theses*. 131.
https://opencommons.uconn.edu/gs_theses/131

This work is brought to you for free and open access by the University of Connecticut Graduate School at OpenCommons@UConn. It has been accepted for inclusion in Master's Theses by an authorized administrator of OpenCommons@UConn. For more information, please contact opencommons@uconn.edu.

**A Comparative Analysis of Different Fields of View in Cone Beam
Computed Tomography Imaging to Identify the Inferior Alveolar Nerve
Canal**

Ibrahim Yamany

BDS, Faculty of Dentistry, King Abdulaziz University, 2004

A Thesis

Submitted in Partial Fulfillment of the

Requirements for the Degree of

Master of Dental Science

at the

University of Connecticut

2011

APPROVAL PAGE

Master of Dental Science Thesis

**A Comparative Analysis of Different Fields of View in Cone Beam
Computed Tomography Images to Identify the Inferior Alveolar Nerve
Canal**

Presented by

Ibrahim Yamany, BDS

Major Advisor _____
Alan G. Lurie, DDS, PhD

Associate Advisor _____
David G. Pendrys, DDS, PhD

Associate Advisor _____
Arthur R. Hand, DDS

**University of Connecticut
2011**

Acknowledgement

I am very grateful to the Almighty God for giving me this wonderful life and leading me through this journey and for giving me everything in my life.

To my wonderful father that I really missed, even though you are not in this life any more you will always be in my heart and soul. Thank you so much for giving me all that I have and making me what I am right now.

To my amazing mother thank you so much for the sound values and principles of life that you have instilled in me and your love and affection, objective criticism and encouragement that have taken me this far. I will come soon and I will never leave you alone.

To my lovely wife Hazar who has stood by me through thick and thin and loved me unconditionally. I know and appreciate all the difficulties you went through in my educational journey and without your love and support I would not have been able to accomplish half the things I have done so far in my life. I love you and thank you for everything.

To my awesome son Beebo (Sohaib) for filling my life with joy and giving me reasons to work hard and continue what my father did and pass everything to you.

I would like to deeply thank Dr. Alan Lurie for the unlimited support and help. Thank you for giving me the chance to come to study in the United States. Thank you for bringing me to the University of Connecticut. I will be forever grateful to you for everything you have done for me since my arrival here. Thank you for being such a wonderful outstanding teacher, your positive attitude and passion has taught us all a lot. You are more than a teacher and program director to me, I see you as a part of my family. I would like to thank you for inspiring and encouraging me to accomplish all that I was able to do during my time at the health center.

To Dr. Kannan Rengasamy for his constant encouragement and advice. I have learnt a lot from our sessions, thank you for being such a wonderful teacher. Thank you for being part of thesis research work. Your motivation and attitude brings a lot of positive energy into the clinic. Thank you for standing by me during my tough times here, I will forever remember you as a wonderful person and a very dear friend.

To Dr. Sanjay Mallya for introducing me to the world of research, the long hours he has spent with me to teach me the fundamentals radiation physics and his contributions to my future career.

To Susan Kirchhoff for all the love and support during the difficult times. The amazing cakes and baked goods made many birthdays - happy. Thank you for everything.

To my dear radiology technologists, the ever-cheerful Melanie Bergmark and Rebecca Santanella without whom the clinic would not have been half as enjoyable. Thank you both for all the wonderful times.

I would like to thank my co-residents (Adi, Rodrigo, Jay, Reji Lakshmi, Asma, Alejandro, Aniket and Hanadi); I really had nice times with all of you. I know at one point of time we will all go to different places but you will always be my closest friends and I am always waiting to hear all the best about your futures.

To Dr. Somerville for being such a good friend and teaching me hints about implant dentistry and giving me the permission to work with the CBCT unit to complete my research projects - your help and support are invaluable.

To Dr. David Pendrys, for introducing me to the powerful world of epidemiology and biostatistics, thank you for participating in this project, thank you for being such an understanding teacher, your attention to every detail, your critical analysis of the scientific process and creative insight into interpreting the data as well as your help in preparing this manuscript, made this project possible. I enjoyed all our discussions while working on this project.

I am very thankful to Dr. Arthur Hand for being such a good teacher. I will never forget your amazing oral histology course, I have learnt a lot from you. Maybe I did not get many chances to work more with you but I am really honored to have you in my thesis committee as an advisor. I will be more honored when I publish this work and have my name next to the name of a pioneer researcher like yourself.

Table of Contents

Acknowledgements	iii
Table of Contents	v
List of Tables	vi
List of Figures	vii
Introduction	1
Hypothesis	11
Specific Aim	11
Significance	11
Materials and Methods	12
Results	24
Discussion	34
Conclusion	44
References	45

List of Tables

Table I: Codes generated for the de-identification of all images.

Table II: Values of the Sensitivity, Specificity, Positive Predictive value (PPV) and Negative Predictive value (NPV) for all field of view.

Table III: Values of areas under the ROC curves for the 6,9, and 12-inch fields of view.

Table IV: Different values of sensitivity and specificity used by the SPSS to plot the ROC curves.

Table V: Values of areas under the ROC curves for the 6,9, and 12-inch fields of view from the first reader in our study.

Table VI: Values of areas under the ROC curves for the 6,9, and 12-inch fields of view from the second reader in our study.

Table VII: Different values of sensitivity and specificity used by the SPSS to plot the ROC curves from the reading of the first reader in the study.

Table VIII: Different values of sensitivity and specificity used by the SPSS to plot the ROC curves from the reading of the second reader in the study.

Table IX: Comparison of the values of areas under 6-inch fields of view ROC curves from the 2 readers in our study.

Table X: Comparison of the values of areas under 9-inch fields of view ROC curves from the 2 readers in our study.

Table XI: Comparison of the values of areas under 12-inch fields of view ROC curves from the 2 readers in our study.

Table XII: Measure of the kappa value for the inter-observer's agreement.

Table XIII: Comparison of the effective doses of different imaging modalities used in the maxillofacial area including Panoramic (OrthoPhos Plus DS), medical CT and samples of CBCT units (CB Mercuray CBCT, i-CAT CBCT, NewTom 3G CBCT, NewTom 9000 and Galileos).

List of Figures

Figure 1: a) reconstructed panoramic image from a CT scan that was done for a 38 year old female showing the root canal filling material inside the IANC. b) the 3-D volume rendered image of the same patient. c) cross sections at mental foramen and the IANC showing the root canal filling material inside the canal.

Figure 2: The plastic container filled with water while the mandible was placed inside to simulate soft tissue attenuation. The contours of the container are similar to the external outline of the mandible.

Figure 3: cross sections through one of our gold standard images. The canal in this case is not defined.

Figure 4: The NiTi orthodontic wires were placed inside the mandibular canals through the mandibular foramina.

Figure 5: 3-D volume rendering showing the orthodontic wires are running in the IANC to the level of the mental foramina. (b) the reconstructed panoramic image showing the wires are running inside the canal.

Figure 6: a) 3-D volume rendering showing the random pathway that the orthodontic wire has taken inside the jaw due to the loss of cortication of the canal walls. This also can be seen on the reconstructed panoramic image (b).

Figure 7: Reconstructed thin-slice panoramic image section showing both canals well defined but one canal (left) with wire running all the way to the level of the mental foramen and the other (right) wire is not running all the way to the mental foramen.

Figure 8: The Receiver Operating Characteristics (ROC) Curve for the 6, 9 and 12-inch fields of view for detection of the mandibular canal.

Figure 9: The Receiver Operating Characteristics (ROC) Curve for the 6, 9 and 12-inch fields of view for detection of the mandibular canal from the first reader in our study.

Figure 10: The Receiver Operating Characteristics (ROC) Curve for the 6, 9 and 12-inch fields of view for detection of the mandibular canal from the second reader in our study.

Figure 11: The reader's agreement / disagreement pie chart.

Figure 12: The reader's disagreement pie chart.

Figure 13: The Receiver Operating Characteristics (ROC) Curve for the 6-inch field of view for detection of the mandibular canal for both readers in our study.

Figure 14: The Receiver Operating Characteristics (ROC) Curve for the 9-inch field of view for detection of the mandibular canal for both readers in our study.

Figure 15: The Receiver Operating Characteristics (ROC) Curve for the 12-inch field of view for detection of the mandibular canal for both readers in our study.

Introduction

The inferior alveolar nerve canal (IANC) a bony canal containing the inferior alveolar nerve (IAN), is a critical structure in many dental procedures, including exodontia, orthognathic surgery and dental implant placement. The canals are located in both sides of the mandible. They start from the mandibular foramina, located on the medial surfaces of the mandibular rami, and run inferiorly and anteriorly toward the mandibular bodies. They continue in the mandibular bodies and run anteriorly and gradually laterally (buccally) until they exit the mandibular bodies at the buccal surfaces through the mental foramina. Anatomical variations occur concerning the location of the mental foramen (1, 2). It is usually found more coronal than the mandibular canal (3, 4). Agthong et al. (5) found that the mental foramen was 28 mm lateral to the midline of the mandible and 14 to 15 mm superior to the inferior border of the mandible. Similarly, Neiva et al. (6) reported that the mental foramen was 27.6 mm (range: 22 to 31 mm) from the midline and 12mm (range: 9 to 15 mm) superior to the most apical portion of the lower cortex of the mandible. Other authors (7) expressed the position of the mental foramen in terms of its location in relation to the inferior border of the mandible and the crest of alveolar bone. The authors thought the mental foramen was usually found halfway between the crest of bone and the inferior border of the mandible. However, this finding can be influenced by periodontal disease and the amount of crestal bone loss. The mental foramen is usually located near the apex of the second mandibular premolar or between the apices of the premolars, and may be either round or ovoid. Minor variations may be race related (8). The IANC is also known as the mandibular canal; in this study both names might be used. Inside the IANC run the IAN, inferior alveolar artery and inferior

alveolar vein. IAN (also sometimes known as the inferior dental nerve) is a branch of the mandibular nerve, which is itself the third branch (V3) of the trigeminal nerve (cranial nerve V). While running in the IANC within the mandible, the IAN supplies the mandibular teeth with sensory branches that form into the inferior dental plexus and give off small gingival and dental nerves to the teeth. Anteriorly, the IAN gives off the mental nerve, which exits the mandible via the mental foramen and supplies sensory branches to the chin, lower lip and gingiva anterior to the mental foramen. The IAN continues anteriorly as the mandibular incisive nerve in the incisive canal (8) to innervate the mandibular canines and incisors. A variation of the IAN with clinical significance in case of any surgical procedures at the premolar/canine area is the anterior loop, which is an extension of the IAN anterior to the mental foramen prior exiting the canal (3, 8).

The inferior alveolar artery is a branch of the maxillary artery that accompanies the IAN in the mandibular canal and divides into two branches, incisor and mental. The incisor branch continues forward beneath the incisor teeth as far as the midline, where it anastomoses with the incisor branch of the opposite side. The inferior alveolar artery and its incisor branch during their course through the substance of the bone give off a few twigs which are lost in the cancellous tissue, and a series of branches which correspond in number to the roots of the teeth: these enter the minute apertures at the apices of the roots and supply the pulps of the teeth. The mental branch exits the mandible with the nerve at the mental foramen, supplies the chin, and anastomoses with the submental and inferior labial arteries. Before the artery enters the mandibular canal it gives off a mylohyoid branch, which supplies the mylohyoid muscle. The inferior alveolar vein is a tributary of

the pterygoid plexus that accompanies the inferior alveolar artery and drains the mandibular teeth. It is the most superior structure running in the IANC (9). Thus, it is clear that the IANC is a vital structure, hosting a crucial neurologic innervation and blood supply to the lower teeth, lip and chin.

A study was conducted by Levine et al. (10) to measure the position of the IANC at the level of first molar and to identify variables that may be associated with the position of the IANC. Direct buccal linear measurement was made from the buccal cortical margin of the IANC to the lateral (buccal) cortical margin of the mandible and direct vertical linear measurement was also made from the alveolar crest to the superior aspect of the IANC. They concluded that the IANC was 4.9 mm and 17.4 mm from the buccal and superior cortical surfaces of the mandible, respectively. The bucco-lingual IANC position was associated with age and race. Older patients and white patients, on average, have less distance between the buccal aspect of the canal and the buccal mandibular border.

The IANC runs in proximity to the apices of the mandibular molars and premolars. Root apices of the mandibular second molars are closer to the mandibular canal than are the root apices of other teeth. The mesial root of the second molar is closer to the IAN in female patients when compared with male patients. Root apices in younger patients (<18 years) are generally closer to the IANC than in older patients (11). Careful attention should be paid to the IANC when any kind of treatment is to be performed in its vicinity. Commonly performed treatments in these areas include endodontic therapy, extractions, excision of broken down and impacted teeth, excision of cysts and tumors, dental implant

placement and placement of screws and bone plates during open reduction of mandibular fractures and orthognathic surgery.

Endodontic therapy might damage the IAN by several mechanisms including (12) neurotoxic effect as a result of root canal filling material penetrating the IANC (13, 14); mechanical pressure or trauma on the nerve caused by overextension of filling material or over-instrumentation with hand or rotary files (13, 14); or (15) an increase in temperature near the IAN greater than 10°C (14). It has been suggested that IAN damage occurs during 1% of mandibular premolar endodontic therapy (14). An example of trauma is a 38 year-old female patient who presented to the endodontic clinic at the University of Connecticut School of Dental Medicine with a chief complaint “I have continuous pain in the lower left side”. She had a history of root canal treatment in a lower left molar 3 weeks prior to the clinical presentation, and a medical CT exam revealed that tooth # 20 had undergone root canal treatment with endodontic filling material beyond the root apex, penetrating the IANC (Figure 1).

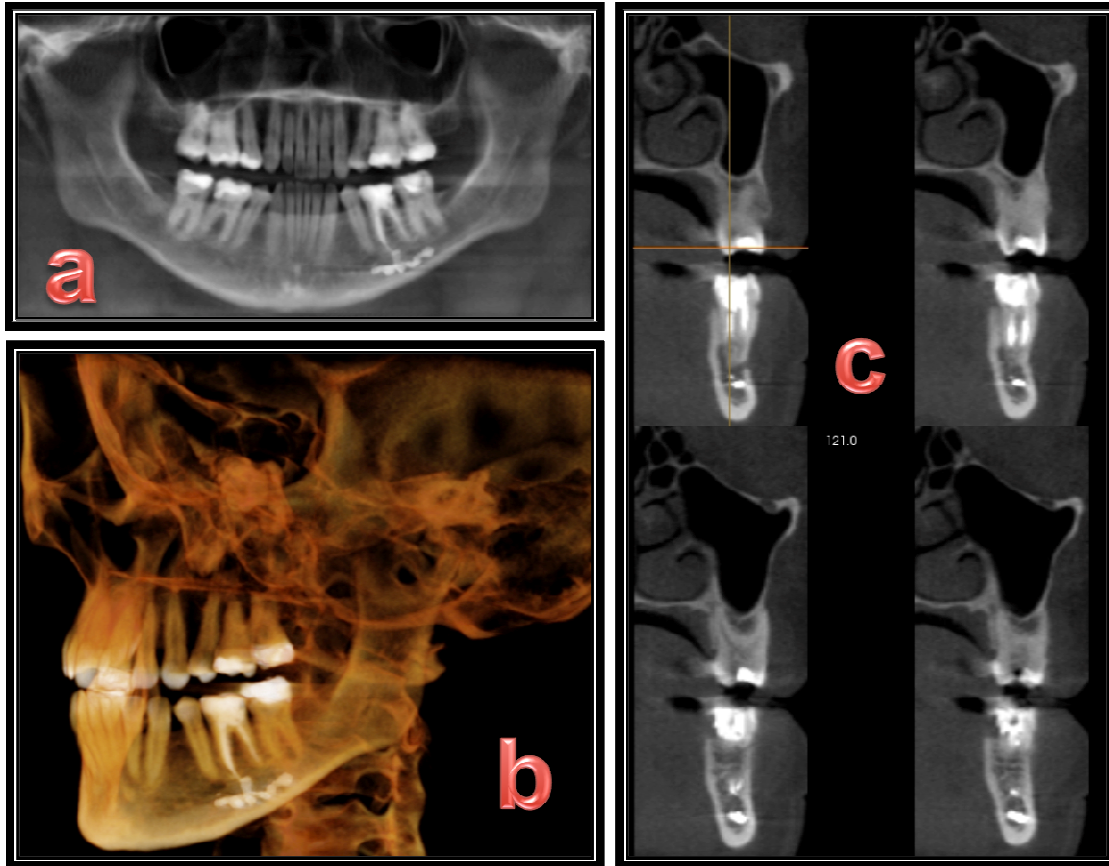


Figure 1: a) reconstructed panoramic image from a CT scan that was done for a 38 year old female showing the root canal filling material inside the IANC. b) the 3-D volume rendered image of the same patient. c) cross sections at mental foramen and the IANC showing the root canal filling material inside the canal. (Courtesy the Endodontolgy Division at the University of Connecticut, School of Dental Medicine)

A close relationship between the roots of the mandibular third molars and the IANC is a common occurrence. This places the IANC at risk of damage during extraction of such teeth. The incidence of damage to the IAN after mandibular third molar extraction ranges from 0.5% (16) to approximately 8 % (17, 18). Factors including age of the patient, experience of the surgeon and depth of the impaction in the bone influence the risk for IAN damage (19, 20). It is also possible for cysts and tumors in the mandible to have

intimate relation with the IANC and in such cases proper planning of the surgical approach to treat these cases is critical.

Dental implants are now increasingly used for replacement of missing teeth. When placing dental implants in the mandibular molar and premolar areas there is always a possibility of traumatizing the IANC, especially with reduced height of the residual ridge frequently found in edentulous areas. Screws that are placed during surgical open fracture reduction or orthognathic surgery may also cause damage to the IAN if placed inside the mandibular canal.

Violation of the mandibular canal or mental foramen can result in injury of the IAN, mental nerve, or adjacent blood vessels. This might cause paresthesia (numb feeling), hypoesthesia (reduced feeling), hyperesthesia (increased sensitivity), dysesthesia (painful sensation), or anesthesia (complete loss of feeling) of the teeth, the lower lip, or surrounding skin and mucosa (8). It also may result in venous or arterial bleeding.

Additional terms used to describe nerve injuries involve (8).

- Neuropraxia: there is no loss of continuity of the nerve; it has been stretched or undergone blunt trauma; the paresthesia will subside, and feeling will return in days to weeks.
- Axonotmesis: nerve damaged but not severed; feeling returns within 2 to 6 months.
- Neurotmesis: severed nerve, poor prognosis for resolution of paresthesia.

It is clear that proper treatment planning of any dental disease, cyst or tumor in the vicinity of the IANC is crucial for the prevention of IANC injury. Treatment planning would mainly depend on the visibility of the IANC and adjacent structures. The visibility of the canal would basically rely on the imaging modality used during treatment planning and the radiographic appearance of the IANC. Imaging modalities that have been used for such treatment planning and localizing of the IANC include periapical radiographs, panoramic radiographs, computed tomography (CT) and Cone Beam Computed Tomography (CBCT). Panoramic radiography and periapical radiography are 2 dimensional images and this makes them more difficult to interpret. As an example, neither of these 2-D radiographs is helpful for determining the bucco-lingual relations between roots of impacted third molars and the IANC. If occlusal radiographs were used to assist in the visibility of the IANC in the axial plane, mandibular molars and premolars would overlap and obscure the IANC. Intraoral radiographs with vertical shift might help in localization but they are not accurate in giving precise measurements (21). For many years in such clinical situations where three-dimensional images are needed, a medical CT had been the only choice. The high cost, radiation dose and limited accessibility restricted its use in routine dentistry. In addition, the medical CT images did not completely satisfy the treatment planning needs of the dentist due to the unavailability of dentist-friendly software programs that allow dentists to perform specific dental treatment planning procedures on the images such as IANC tracing and simulation of implant fixture placements.

The invention of CBCT, with its substantially lower radiation dose compared to medical CT (22), lower cost, better accessibility and associated software programs specifically designed for use in dental diagnosis and treatment planning, made the possibility of examining the canal in three dimensions more feasible for dentists. Although the CBCT principle has been in use for almost 2 decades, CBCT machines have not been used in dental practice until 2001. This was due to the development of inexpensive x-ray tubes, high-quality detector systems, powerful personal computers and reduced cost and field-of-view CBCT systems becoming commercially available. NewTom QR DVT 9000 (Quantitative Radiology s.r.l. Verona, Italy) 4 was introduced in April 2001; other units include CB MercuRay (Hitachi Medical Corp., Kashiwa-shi, Chiba-ken, Japan), 3D Accuitomo – XYZ Slice View Tomograph (J. Morita Mfg Corp., Kyoto, Japan) and i-CAT (Xoran Technologies, Ann Arbor, Mich., and Imaging Sciences International, Hatfield, PA). There are many recently released CBCT machines and their use in dentistry is accelerating rapidly (23).

CBCT units are based on volumetric tomography, using a 2 dimensional extended digital array providing an area detector. This is combined with a cone shaped x-ray beam. The cone-beam technique consists of a single 360° scan in which the x-ray source and a reciprocating detector synchronously rotate around the patient's head; the head is stabilized or supported with a head holder or rest. At certain degree intervals, single projection images are acquired (known as “basis” images). These are similar to lateral cephalometric radiographic images, each slightly offset from one another. This series of basis projection images is known as the projection data. Software programs incorporating

sophisticated algorithms including back-filtered projection are applied to projection data to generate a 3 dimensional volumetric data set that can be used to provide primary reconstruction images in 3 orthogonal planes (axial, sagittal and coronal) (24).

There are mainly 2 types of x-ray detectors used in CBCT units (25, 26). The first is the image intensifier tube / charge-coupled device combination detector. The second is the flat panel detector that was released by (i-CAT) (27). The flat panel detector consists of a cesium iodide scintillator applied to a thin film transistor made of amorphous silicon.

Images produced by an image intensifier tube / charge-coupled device combination have lower signal to noise ratio than images from a flat panel detector (23). The field of view (FOV) of a CBCT system or the scan volume represents the dimensions of the area of the patient to be covered by the scan. Its size varies from one CBCT unit to another and its shape might be either cylindrical or spherical. The scan volume depends mainly on the size and shape of the detector, beam projection geometry and the beam collimation. The flexibility in changing the FOV gives the advantage that only the area of interest is exposed to the x-ray beam and avoids unnecessary exposure to other areas. Ability to control the size allows imaging smaller and larger areas of the maxillofacial region (24).

In CBCT units increasing the size of the FOV is usually associated with reduction in the resolution of the image. This is due to the fact that increasing the size of the FOV is inherently associated with an increase in the voxel size since the number of pixels on the detector is fixed. Recently some CBCT units offer the advantage of maintaining resolution of images with increasing size of the FOV. This is basically due to the ability to control the image voxel size in these CBCT units, in a way that the size of the FOV

can be increased and the voxel size is adjusted to a small voxel size or in other words they keep the same voxel size in smaller FOVs (28).

Patel S et al. (29) have studied the potential applications of CBCT in managing patients with endodontic pathology and concluded that CBCT is helpful for clear visualization of the relationships of the root apices to various neighboring anatomic structures such as the mandibular canals and the maxillary sinuses. This would clearly have an impact on the treatment planning and the prognosis of teeth with endodontic pathology. It also has been shown that CBCT depicts the mandibular canal better than panoramic radiography. This is because of the fact that the CBCT images are free of magnification, superimposition of neighboring structures, and other problems inherent to panoramic radiography (30).

CBCT also was compared with the multislice CT in detecting the mandibular neurovascular canal structures such as bifid mandibular canal, accessory mental and buccal foramina, and results showed consistency between the two modalities (31).

Hypothesis

CBCT has high sensitivity and specificity in determination of the position of the inferior alveolar nerve canal (IANC), which diminishes with increasing size of the Field of View (FOV) in CBCT units where the voxel size is not adjustable.

Specific Aim

Define the FOV with the most diagnostically efficacious demonstration of the IANC.

Significance

This could increase quality of patient care by allowing the treating doctor to avoid iatrogenic events involving the neurovascular structures in the IANC.

Materials and Methods

Radiographic exam (scanning): Thirty dry skulls, randomly selected, were borrowed from the University of Connecticut's Department of Education support Services. Age, gender and race of the skulls used for the study were unknown. From the selected specimen skulls for the study, mandibles were detached for imaging. Mandibles were placed in a thin, clear plastic container that has an outline similar to the outer surface of the mandible and surrounds the mandibles with even distances bilaterally in the range of 0.2 to 0.7 inch depending on the size of the mandible (Figure 2). The container was filled with water to simulate soft tissue attenuation. To ensure that air bubbles were not accumulated inside the bone marrow spaces and IANCs after immersing of the mandibles in the water, a plastic syringe was used to inject water into the IANC through the mandibular foramen.

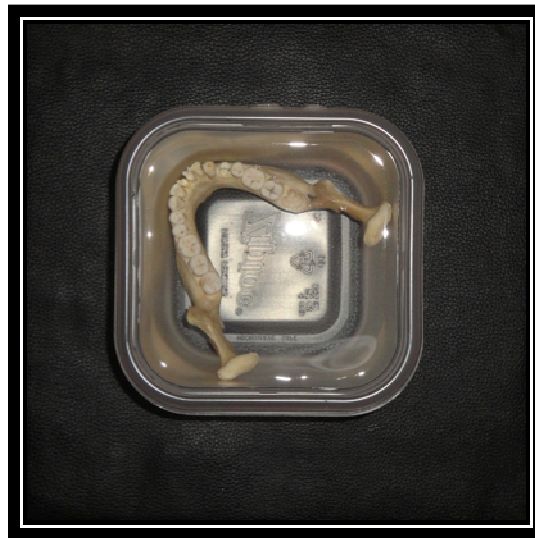


Figure 2: The plastic container filled with water while the mandible was placed inside to simulate soft tissue attenuation. The contours of the container are similar to the external outline of the mandible.

All mandibles were imaged with the Hitachi CB MercuRay (Hitachi Medico Technology, Tokyo, Japan) CBCT unit at the University of Connecticut Health Center using the standard departmental protocol of 120 KV and 15 mA. The unit has three FOVs; 6, 9 and 12-inches with spherical scan volume shapes. Each mandible was imaged three times, one image with each FOV on this CBCT machine. The mandibles were carefully placed in the FOV before imaging using the positioning guides to ensure that both IANCs were seen in the images. The unit acquires 288 projected images, each of which consists of 512 x 512 matrices and 12-bits grey depth. Following this, 3D (volume) data are reconstructed using a proprietary Hitachi parallel processing system designed specifically for this instrument. The projection data are corrected using calibration data generated from the detector's response to a scan of air. Geometrical distortion of the image intensifier is then corrected using a correction table for distortion of the image intensifier. Based on these corrected projection data, CT images are reconstructed according to the cone beam backprojection method proposed by Feldkamp et al. (32). A total of 512 axial images are produced and saved in the original format but they can also be exported in DICOM format. Reconstruction of images from projected images takes approximately 5 minutes (33). All images were reconstructed on CBWorks 2.0 software (Cybermed Corp., Seoul, Korea). All generated DICOM data were saved in a Seagate FreeAgent Go 500 GB USB 2.0 Portable External Hard Drive.

Before imaging of the mandibles each image was assigned an identification code that was unknown to the oral and maxillofacial (OMF) radiologist reviewing the images. Each code was composed of three randomly generated letters (Table I). During registration of

each image the gender was selected to be unspecified and all images were given the same date of birth.

Skull	Code	Skull	Code	Skull	Code	Skull	Code
1 6"	NUZ	9 6"	YBK	17 6"	WCI	25 6"	URG
1 9"	JPV	9 9"	ZAL	17 9"	XDJ	25 9"	VQH
1 12"	LPX	9 12"	AAM	17 12"	YEK	25 12"	WPI
2 6"	DKP	10 6"	BZN	18 6"	ZFL	26 6"	XOJ
2 9"	ELQ	10 9"	CYO	18 9"	AGM	26 9"	YNK
2 12"	LSX	10 12"	DXP	18 12"	BHN	26 12"	ZML
3 6"	GNS	11 6"	EWQ	19 6"	CIO	27 6"	ALM
3 9"	HOT	11 9"	FVR	19 9"	DJP	27 9"	BKN
3 12"	IPU	11 12"	GUS	19 12"	JRV	27 12"	CMO
4 6"	JQV	12 6"	HTT	20 6"	FLR	28 6"	DIP
4 9"	KRW	12 9"	ISU	20 9"	GMS	28 9"	EHQ
4 12"	AHM	12 12"	EKQ	20 12"	HNT	28 12"	FGR
5 6"	MTY	13 6"	KQW	21 6"	IOU	29 6"	GFS
5 9"	FMR	13 9"	CJO	21 9"	BIN	29 9"	HET
5 12"	OVA	13 12"	MOY	21 12"	KQU	29 12"	IDU
6 6"	PWB	14 6"	NNZ	22 6"	LRX	30 6"	JCV
6 9"	QXC	14 9"	OMA	22 9"	MSY	30 9"	KBW
6 12"	RYD	14 12"	TZF	22 12"	NTZ	30 12"	LAX
7 6"	SZE	15 6"	QKC	23 6"	OUA		
7 9"	TAF	15 9"	RJD	23 9"	PVB		
7 12"	UBG	15 12"	SIE	23 12"	QWC		
8 6"	VCH	16 6"	THF	24 6"	RXD		
8 9"	WDI	16 9"	UGG	24 9"	SYE		
8 12"	XEJ	16 12"	VFH	24 12"	PLB		

Table I: Codes generated for the de-identification of all images.

Radiographic interpretation: Two calibrated OMF radiologists reviewed all images; both of them are diplomates of the American Board of Oral and Maxillofacial Radiology (OMFR). Calibration was done in 3 orientation sessions. The images were reviewed using third party software (InVivoDental software, Anatomage, San Jose, CA), which is widely used for dental implant treatment planning. Images were projected on 3 monitors of the picture archiving and communication system (PACS) workstation in the OMFR reading room at the OMFR clinic in the University of Connecticut School of Dental Medicine. Images were exported from the external hard drive to the Hewlett-Packard xw8200 – Intel – Microsoft windows XP professional, version 2002, computer at the PACS work station and then imported to the InVivoDental software in random order. The examiners reviewed the volumes in ideal dimly lit viewing conditions. Since both examiners are experienced OMF radiologists, they were allowed to handle the volumes freely with the software and use all available tools and instruments to identify the IANC. They were also allowed to change contrast and brightness. We decided to focus on the IANC starting from the distal surface of the first molar to the mental foramen. This was because in practical life the area of the first molar and premolar area is the area where many implants are placed and many dental procedures are performed, including root canal treatments and extractions. Additionally, we noticed that canal is easy to identify in the ramus area and that would have an impact on and bias the results of our study.

The examiners used a five-point scale developed for this study to identify the IANC:

- 1- The canal is definitely not identified
- 2- The canal is probably not identified
- 3- The canal is probably identified

- 4- Part of the canal is definitely identified
- 5- The canal is definitely identified.

Each side of each image was scored separately; this gave a total of sixty canals.

Examiners reviewed the volumes separately and no more than 15 images were reviewed at one session to avoid examiners exhaustion and eye fatigue. The part of the canal that emerges in the buccal cortical plate and is considered part of the mental foramen was not considered during scoring of the canal (Figure 3).

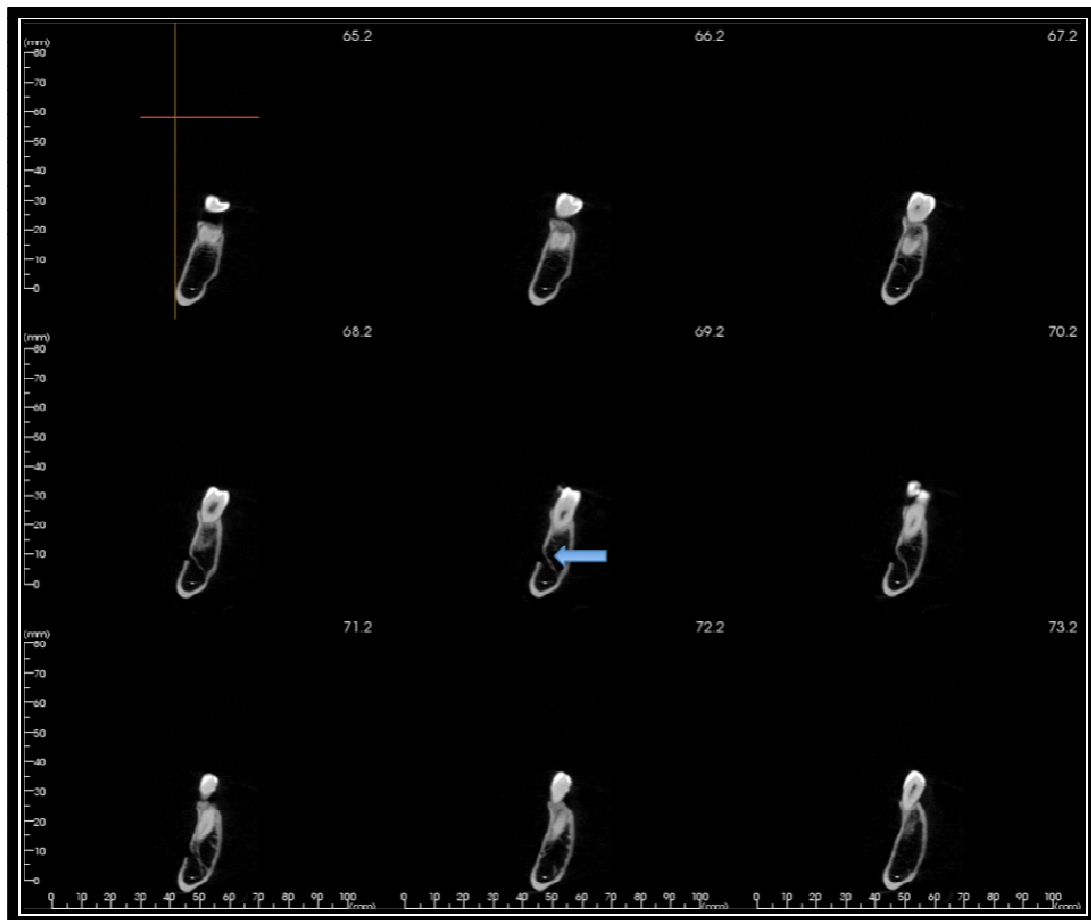


Figure 3: cross sections through one of our gold standard images. The canal in this case is not defined. The arrow is pointing to part of the mental foramen that we did not consider as part of the canal during identification of the canal.

Gold standard: to establish the gold standard for our study, all mandibles were imaged again without soft tissue attenuation. This led to sharper images due to the decrease in amount of scattered radiation and increased the signal: noise ratio plus gave higher contrast between bone marrow spaces filled with air and bone tissues. In addition, a 0.12mm round NiTi orthodontic wire was placed in the IANC starting from the mandibular foramen (Figure 4). The wire helped to locate the canal and prove that what we were identifying was the canal. Unfortunately it is an inherent character of CBCT that metals cause a scatter artifact but this was minimized in our study by using very thin orthodontic wires. In case the IANC was corticated with a definite roof, floor and walls, the wire would run only inside the canal to the level of the mental foramen and the canal would be scored as definitely identified (Figure 5). In other cases the canal has lost its cortical borders and the wire would randomly run in the mandible in a random direction; such a canal would have been scored as definitely not identified (Figure 6). We also noticed in some cases that the wire did not go completely to the mental foramen but the remaining part of the canal was definitely seen in the first molar and premolar area; this case was also scored as “The canal is definitely identified” (Figure 7).



Figure 4: The NiTi orthodontic wires were placed inside the mandibular canals through the mandibular foramina.



Figure 5: a) 3-D volume rendering showing the orthodontic wires are running in the IANC to the level of the mental foramina. b) The reconstructed panoramic image showing the wires are running inside the canal.

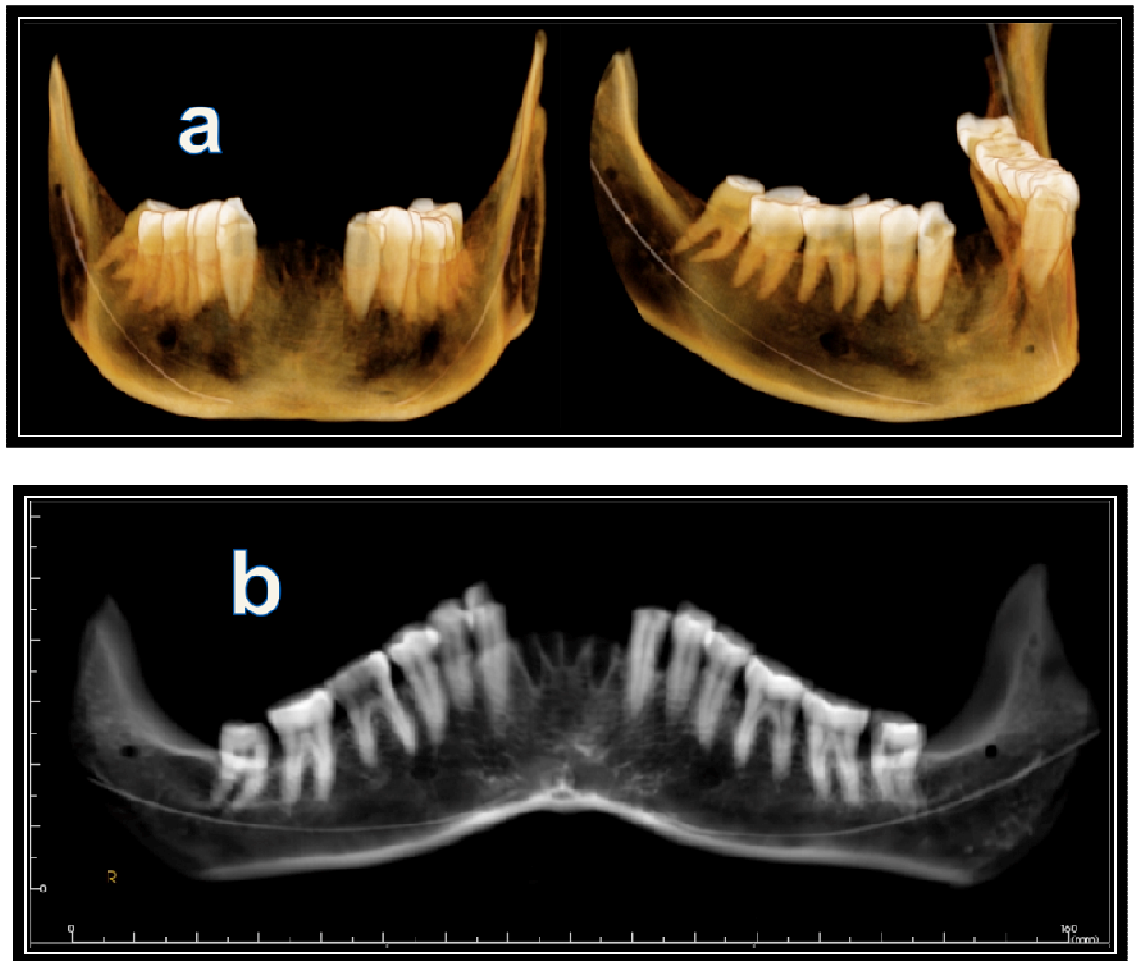


Figure 6: a) 3-D volume rendering showing the random pathway that the orthodontic wire has taken inside the jaw due to the loss of cortication of the canal walls. This also can be seen on the reconstructed panoramic image (b).

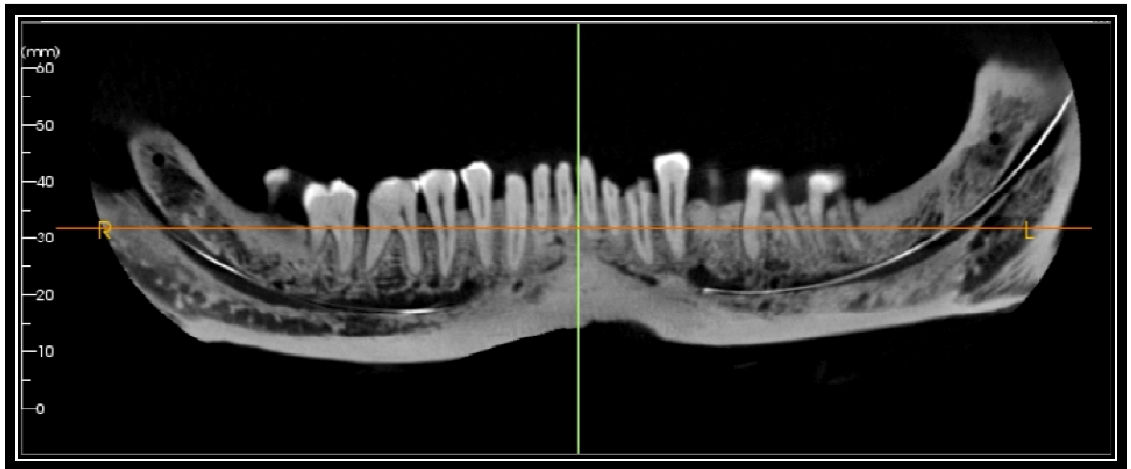


Figure 7: Reconstructed thin-slice panoramic image section showing well defined both canals but one canal (left) with wire running all the way to the level of the mental foramen and the other (right) wire is not running all the way to the mental foramen.

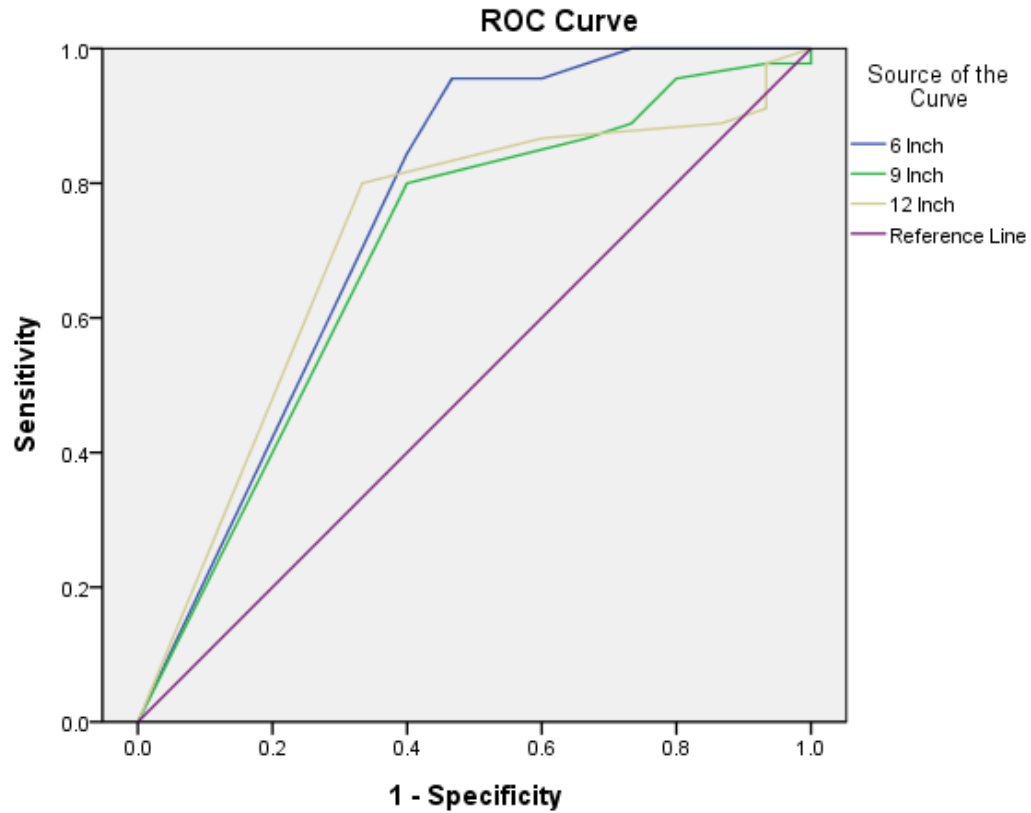
Statistical analysis: The performance of each FOV was evaluated by calculating the sensitivity, specificity, positive predictive value and negative predictive value. We also generated the receiver operating characteristic (ROC) curves for each using the Statistical Package for the Social Sciences (SPSS version 17.0). The areas under the ROC curves were also calculated and the statistical difference between areas under the ROC curves was assessed using a nonparametric test at a confidence level of 95.00%. For the purpose of getting more detailed statistical information about our study we also generated the ROC curves for each reader separately on each FOV. Every ROC of a certain FOV from one reader was also compared to the ROC curve of the same FOV for the other reader. The interobserver agreement was assessed by the calculation of the Cohen kappa statistics with SPSS. Interpretation of the kappa statistics was based on the guidelines of Landis and Koch (34): less than 0 (poor), 0 - 0.20 (slight), 0.21 - 0.40 (fair), 0.41 - 0.60 (moderate), 0.61 - 0.80 (substantial), 0.81 - 1.00 (almost perfect). We also calculated the number of agreements (similar readings) and disagreements (non similar readings) between the two readers. The disagreement was classified into 1, 2, 3 and 4 points by subtracting the lower value reading of the same canal for the same FOV from the higher value reading. The number of each disagreement category was calculated and its percentage to the total number of disagreements was also calculated. Finally, we calculated the mean, median, standard deviation and the mode of the total number of disagreements.

Results

The 6-inch FOV showed sensitivity, specificity, positive predictive value and the negative predictive value equal to 86.36 %, 60.00 %, 84.44 % and 56.25 % respectively. For the 9-inch FOV these values were 80.00 %, 60.00 %, 80.00 % and 50.00 % while values for the 12-inch FOV are 80.00 %, 66.67 %, 87.80 and 52.63 respectively (Table II). The areas under the ROC curves of the 6-inch, 9-inch and the 12-inch FOVs respectively were 0.753, 0.696 and 0.716 (Figure 8). There was no statistically significant difference between the 3 FOVs at a confidence level of 95.00%. It can be seen that the area under the 6-inch FOV, ROC curve had the highest value (Table III). The different values of sensitivity and specificity that were used for plotting the ROC curves are shown in Table IV; the smallest cutoff value is the minimum reading on the test minus 1, and the largest cutoff value is the maximum test reading plus 1. All the other cutoff values are averages of 2 consecutive ordered observed test readings.

Field of View	Sensitivity	Specificity	PPV	NPV
6-inch	86.36 %	60.00 %	84.44 %	56.25 %
9-inch	80.00 %	60.00 %	80.00 %	50.00 %
12-inch	80.00 %	66.67 %	87.80 %	52.63 %

Table II: Values of the Sensitivity, Specificity, Positive Predictive value (PPV) and Negative Predictive value (NPV) for all fields of view.



Diagonal segments are produced by ties.

Figure 8: The Receiver Operating Characteristics (ROC) Curve for the 6, 9 and 12-inch fields of view for detection of the mandibular canal.

Area Under the Curve					
Test Result Variable(s)	Area	Std. Error	Asymptotic Sig.	Asymptotic 95% Confidence Interval	
				Lower Bound	Upper Bound
6 Inch	.753	.085	.004	.588	.919
9 Inch	.696	.083	.024	.534	.859
12 Inch	.716	.079	.013	.560	.871

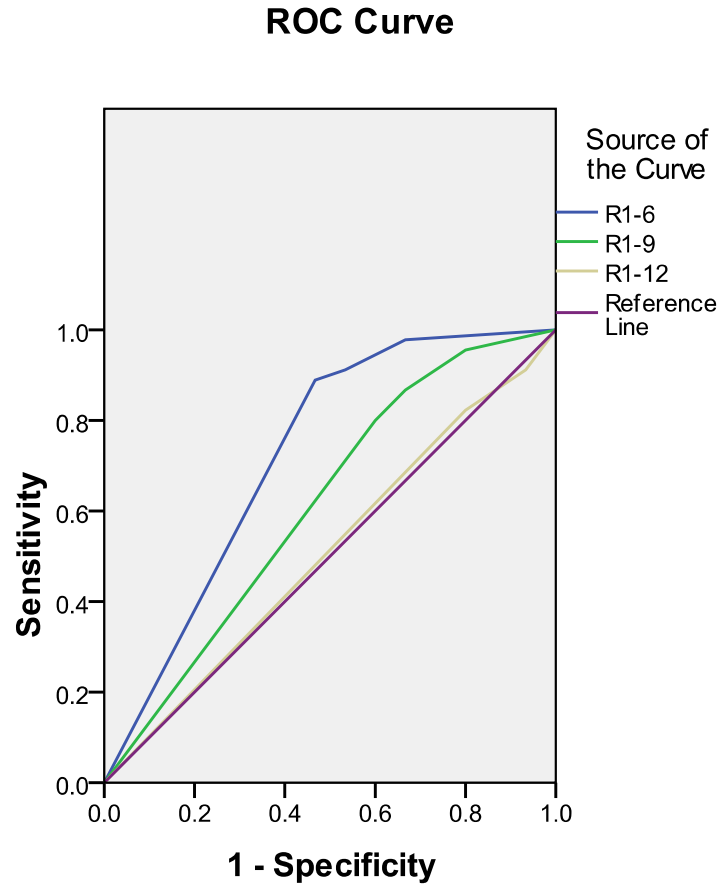
Table III: Values of areas under the ROC curves for the 6,9, and 12-inch fields of view.

Coordinates of the Curve			
Test Result Variable(s)	Positive if Greater Than or Equal To	Sensitivity	1 - Specificity
6 Inch	.50	1.000	1.000
	1.75	1.000	.733
	2.25	.956	.600
	3.00	.956	.467
	4.25	.844	.400
	6.00	.000	.000
9 Inch	.00	1.000	1.000
	1.25	.978	1.000
	1.75	.978	.933
	2.25	.956	.800
	2.75	.889	.733
	3.25	.867	.667
	4.25	.800	.400
	6.00	.000	.000
12 Inch	.50	1.000	1.000
	1.75	.978	.933
	2.25	.911	.933
	2.75	.889	.867
	3.25	.867	.600
	4.25	.800	.333
	6.00	.000	.000

Table IV: Different values of sensitivity and specificity used by the SPSS to plot the ROC curves. The smallest cutoff value is the minimum observed test value minus 1, and the largest cutoff value is the maximum observed test value plus 1. All the other cutoff values are the averages of two consecutive ordered observed test values.

The areas under the ROC curve of the 6-inch, 9-inch and 12-inch for first reader respectively were 0.723, 0.613 and 0.508 (Figure 9). There was also no statistically significant difference between the FOVs but the 6-inch performed better, especially when

compared to the 12-inch FOV; the 12-inch FOV was similar to tossing a coin (Table V). The values of the second reader's areas under the ROC curve for the 6-inch, 9-inch and 12-inch FOVs respectively were 0.817, 0.772 and 0.705 (Figure 10) with no statistically significant difference between the areas at a confidence level of 95.00 % (Table VI). It is noted that the second reader shower higher values of the areas under the ROC curves. The different values of sensitivity and specificity that were used for plotting the ROC curves for both readers are shown in Tables VII and VIII. The smallest cutoff value is the minimum test minus 1, and the largest cutoff value is the maximum reading of the test plus 1 while all the other cutoff values are averages of 2 consecutive ordered observed test readings.



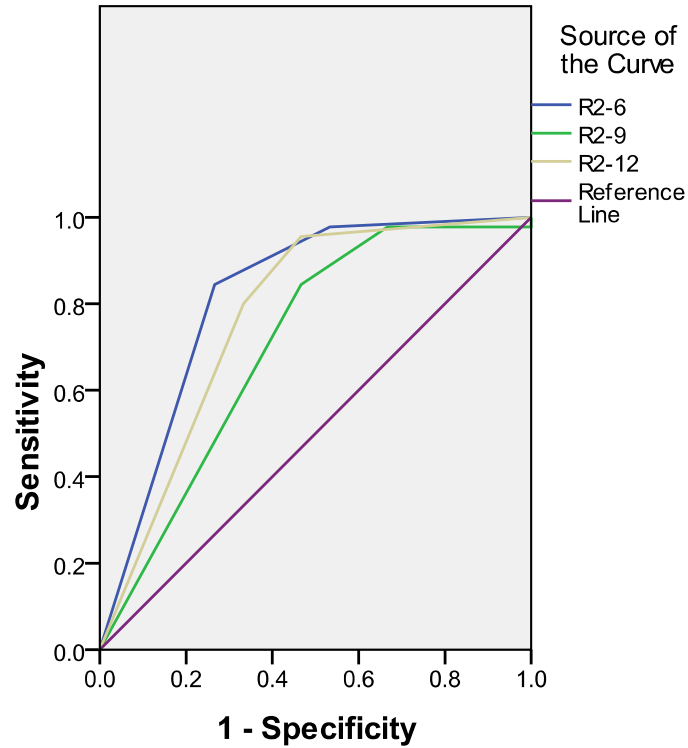
Diagonal segments are produced by ties.

Figure 9: The Receiver Operating Characteristics (ROC) Curve for the 6, 9 and 12-inch fields of view for detection of the mandibular canal from the first reader in our study.

Area Under the Curve					
Test Result Variable(s)	Area	Std. Error	Asymptotic Sig.	Asymptotic 95% Confidence Interval	
				Lower Bound	Upper Bound
R1-6	.723	.086	.010	.554	.892
R1-9	.613	.090	.194	.436	.789
R1-12	.508	.087	.925	.338	.678

Table V: Values of areas under the ROC curves for the 6,9, and 12-inch fields of view from the first reader in our study.

ROC Curve



Diagonal segments are produced by ties.

Figure 10: The Receiver Operating Characteristics (ROC) Curve for the 6, 9 and 12-inch fields of view for detection of the mandibular canal from the second reader in our study.

Area Under the Curve

Test Result Variable(s)	Area	Std. Error	Asymptotic Sig.	Asymptotic 95% Confidence Interval	
				Lower Bound	Upper Bound
R2-6	.817	.074	.000	.672	.962
R2-9	.705	.087	.018	.535	.876
R2-12	.772	.081	.002	.613	.931

Table VI: Values of areas under the ROC curves for the 6,9, and 12-inch fields of view from the second reader in our study.

Coordinates of the Curve			
Test Result Variable(s)	Positive if Greater Than or Equal To	Sensitivity	1 - Specificity
R1-6	.00	1.000	1.000
	1.50	.978	.667
	2.50	.911	.533
	4.00	.889	.467
	6.00	.000	.000
R1-9	.00	1.000	1.000
	1.50	.956	.800
	2.50	.867	.667
	4.00	.800	.600
	6.00	.000	.000
R1-12	.00	1.000	1.000
	1.50	.911	.933
	2.50	.867	.867
	4.00	.822	.800
	6.00	.000	.000

Table VII: Different values of sensitivity and specificity used by the SPSS to plot the ROC curves from the reading of the first reader in the study. The smallest cutoff value is the minimum observed test value minus 1, and the largest cutoff value is the maximum observed test value plus 1. All the other cutoff values are the averages of two consecutive ordered observed test values.

Coordinates of the Curve			
Test Result Variable(s)	Positive if Greater Than or Equal To	Sensitivity	1 - Specificity
R2-6	1.00	1.000	1.000
	2.50	.978	.533
	4.00	.844	.267
	6.00	.000	.000
R2-9	.00	1.000	1.000
	1.50	.978	1.000
	2.50	.978	.667
	4.00	.844	.467
	6.00	.000	.000
R2-12	1.00	1.000	1.000
	2.50	.956	.467
	4.00	.800	.333
	6.00	.000	.000

Table VIII: Different values of sensitivity and specificity used by the SPSS to plot the ROC curves from the reading of the second reader in the study. The smallest cutoff value is the minimum observed test value minus 1, and the largest cutoff value is the maximum observed test value plus 1. All the other cutoff values are the averages of two consecutive ordered observed test values.

The interobserver agreement came out to be fair agreement (kappa score = 0.273) based on the kappa interpretation scale (34). The number of disagreements between the readers was 69 readings out of 180 readings, which represents 38.33 % of the total readings (Figure 11). The number of disagreements in which the difference in the 2 readers' variability is 1 point was 34 out of 69 total number of disagreements, while it was 21 disagreements of 2 point differences and 14 of 3 point differences. No 4 point differences were found. The percentages of 1, 2, 3 and 4 point disagreements to the total number of disagreements respectively are 49.27 %, 30.43 %, 20.28 % and 0.00 % percent (Figure 12). The median of the disagreements was 2 and the mean was 1.71 with standard deviation of 0.787 while the mode was 1.

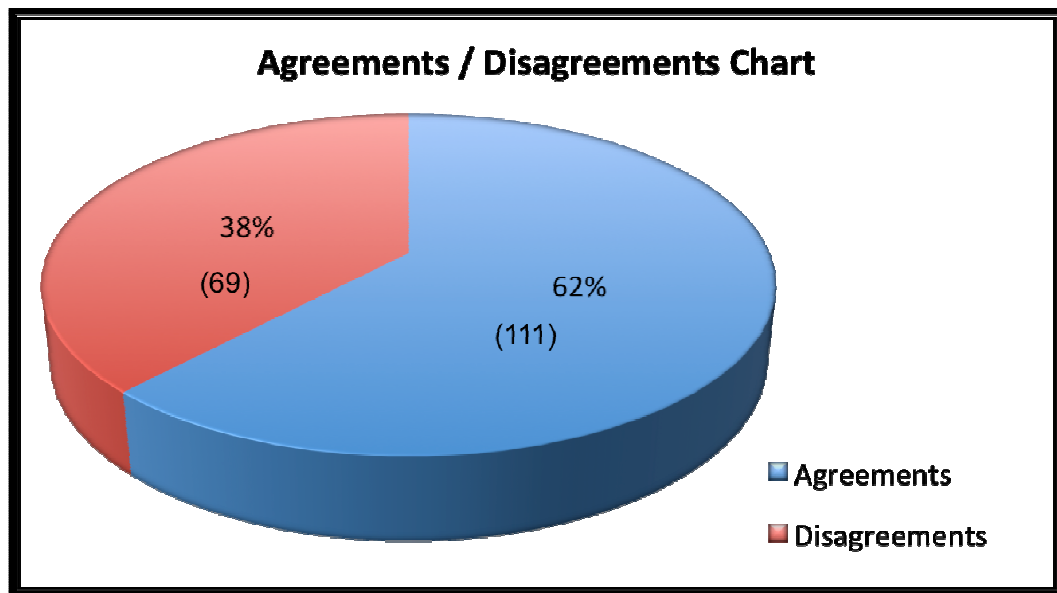


Figure 11: The reader's agreement / disagreement pie chart.

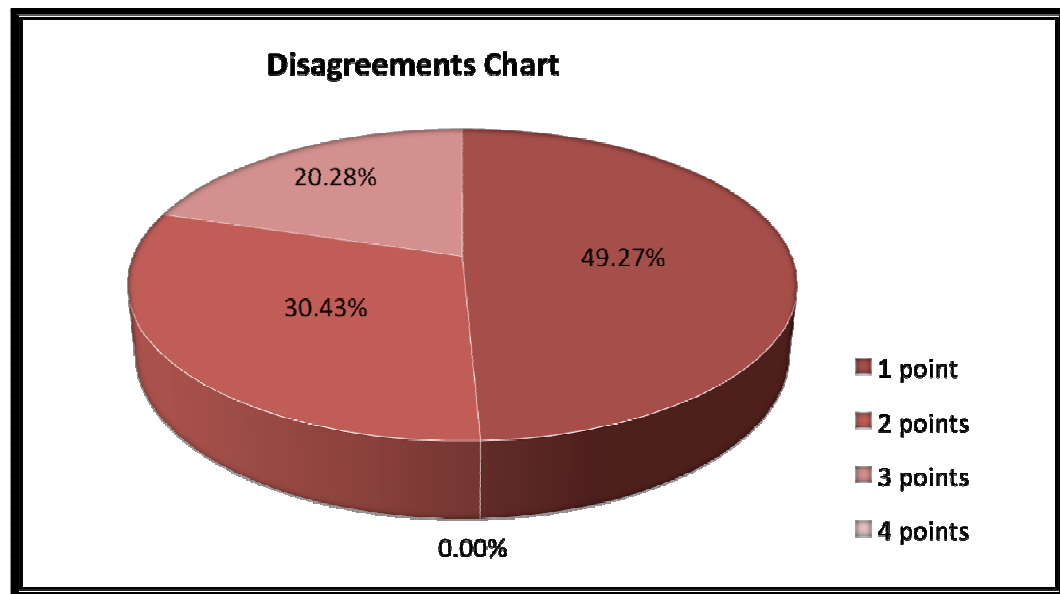


Figure 12: The reader's disagreement pie chart.

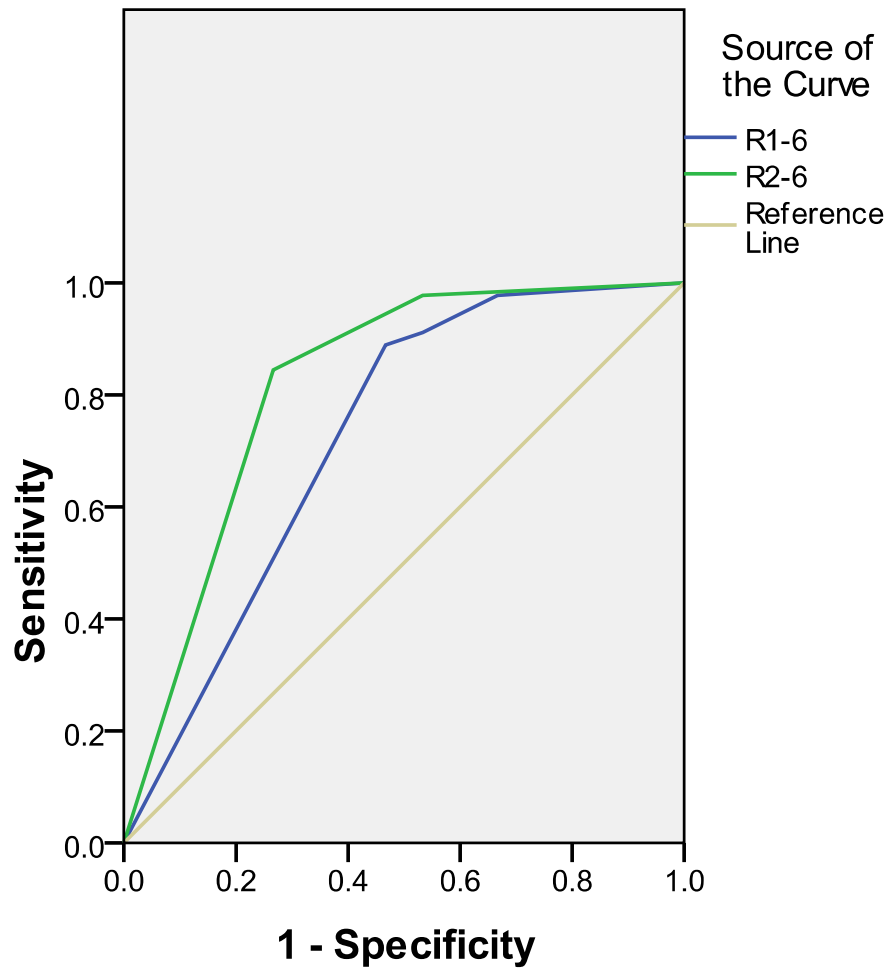
Discussion

The imaging of the IANC with maximum visibility of its roof, floor and lateral walls is essential in some dental procedures. These procedures include implant treatment planning, endodontic treatment, open fracture reduction in the mandibular premolar/molar area and mandibular molar extractions. The introduction of CBCT allows us to look at the IANC in 3 dimensions. However, the results of our study suggest that the CBCT is not always the perfect tool for localization and visualization of the IANC. The ability to demonstrate the IANC depends on the degree of cortication of the roof, floor and lateral walls of the canal. This wall cortication can be affected by gender, thyroid disease (35) and age. The results of our study suggest that the 6-inch FOV is the best imaging protocol in this unit for imaging of the IANC. The 6-inch FOV would be followed by the 12-inch and the 9-inch respectively; this does not completely agree with what we anticipated.

The CB Mercuray CBCT unit produces images that consist of 512 x 512 x 512 isotropic voxels. Sizes of the FOV and voxels for each mode are, respectively, 192.5 mm and 0.376 mm in F (12-inch) mode, 150 mm and 0.293 mm in P (9-inch) mode, 102 mm and 0.200 mm in I (6-Inch) mode (33). So it is known that the 6-Inch FOV is the highest resolution among the three FOV by its smallest voxel size. The resolution quality of the 6-inch FOV is followed by the 9-inch and the 12-inch respectively. Even though the 9-inch FOV has better resolution when compared to the 12-inch FOV, our results suggested that 12-inch might be better for detecting the IANC. The fact that the difference between the two protocols was not statistically significant and the values of the areas under the

ROC curves were very close might explain the results that showed that the 12-inch FOV performed better than the 9-inch FOV. Although this might be a reasonable explanation, we thought there might be other reasons for these results. We further investigated our data to explore a possible reason for this paradoxical result; thus, we generated ROC curves for each reader separately and compared them (Figures 13, 14 and 15).

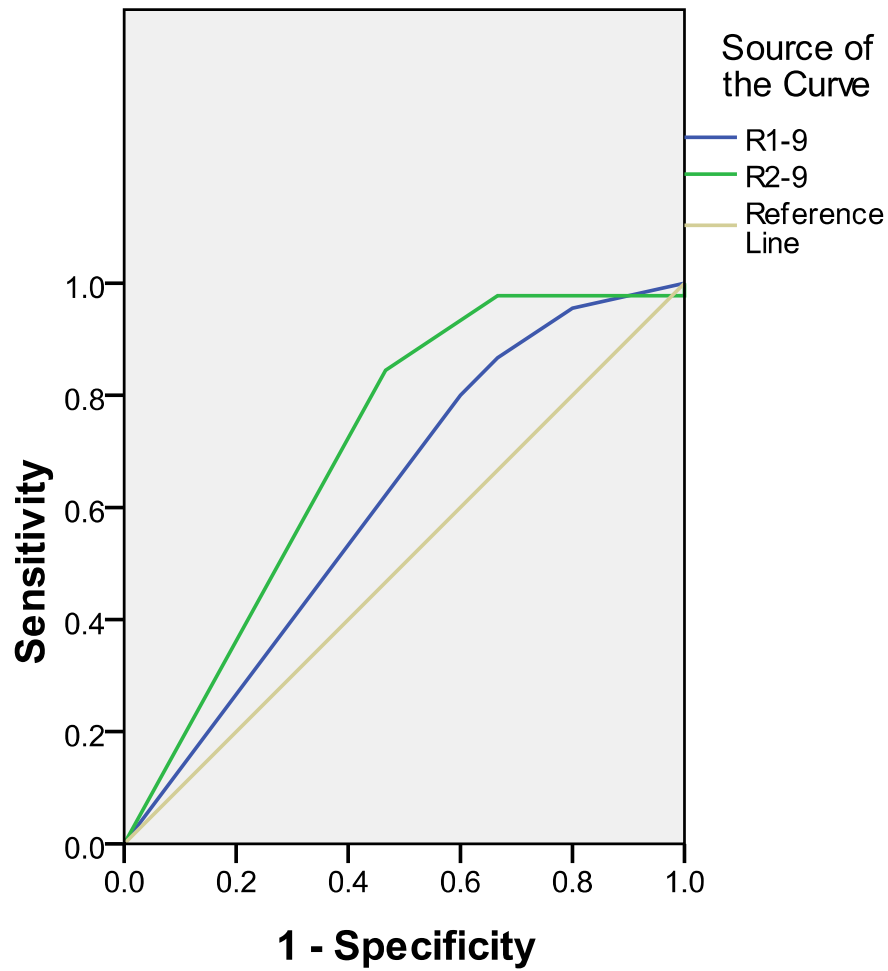
ROC Curve



Diagonal segments are produced by ties.

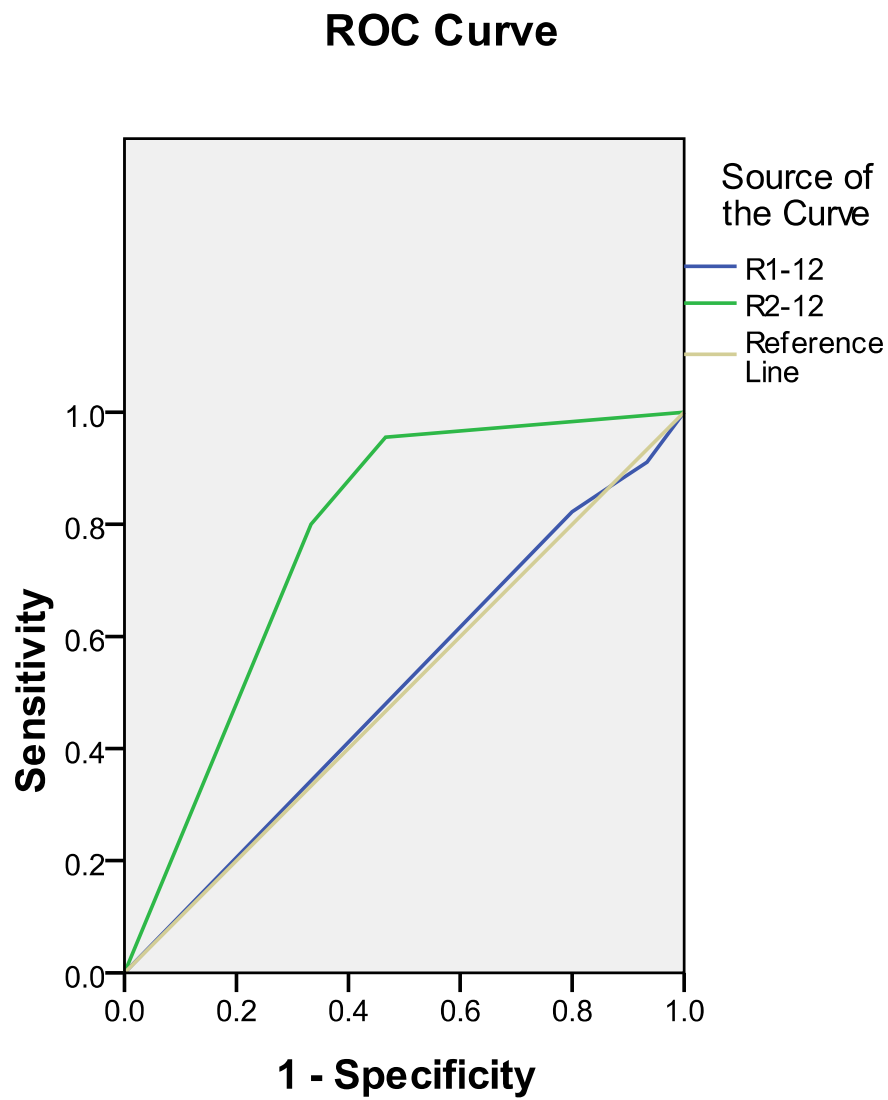
Figure 13: The Receiver Operating Characteristics (ROC) Curve for the 6-inch field of view for detection of the mandibular canal for both readers in our study.

ROC Curve



Diagonal segments are produced by ties.

Figure 14: The Receiver Operating Characteristics (ROC) Curve for the 9-inch field of view for detection of the mandibular canal for both readers in our study.



Diagonal segments are produced by ties.

Figure 15: The Receiver Operating Characteristics (ROC) Curve for the 12-inch field of view for detection of the mandibular canal for both readers in our study.

This analysis showed that one of the two readers had ROC curves with higher values with all FOVs (Tables IX, X and XI). The differences between higher and lower values of the areas under the ROC curves of the two readers were similar differences for both the 6-inch and the 9-inch fields of view. The 12-inch FOV showed greater difference between the 2 values of the areas under the ROC curves when compared to other protocols. The kappa value of the interobserver variability was 0.273; based on the kappa interpretation scale, this is fair agreement. This kappa score, coupled with the high percentages of disagreements between readers (Figures 11 & 12), may explain the finding that the 12-inch FOV performed better than the 9-inch FOV (Table XII).

Area Under the Curve					
Test Result Variable(s)	Area	Std. Error	Asymptotic Sig.	Asymptotic 95% Confidence Interval	
				Lower Bound	Upper Bound
R1-6	.723	.086	.010	.554	.892
R2-6	.817	.074	.000	.672	.962

Table IX: Comparison of the values of areas under 6-inch fields of view ROC curves from the 2 readers in our study.

Area Under the Curve					
Test Result Variable(s)	Area	Std. Error	Asymptotic Sig.	Asymptotic 95% Confidence Interval	
				Lower Bound	Upper Bound
R1-9	.613	.090	.194	.436	.789
R2-9	.705	.087	.018	.535	.876

Table X: Comparison of the values of areas under 9-inch fields of view ROC curves from the 2 readers in our study.

Area Under the Curve					
Test Result Variable(s)	Area	Std. Error	Asymptotic Sig.	Asymptotic 95% Confidence Interval	
				Lower Bound	Upper Bound
R1-12	.508	.087	.925	.338	.678
R2-12	.772	.081	.002	.613	.931

Table XI: Comparison of the values of areas under 12-inch fields of view ROC curves from the 2 readers in our study.

		Value	Asymp. Std. Error	Approx. T	Approx. Sig.
Measure of Agreement	Kappa	.273	.042	6.636	.000
N of Valid Cases		180			

Table XII: Measure of the kappa value for the inter-observer's agreement.

It is known that most radiographic exams are highly susceptible to subjectivity from the individual interpreting them due to the fact that most radiographic exams don't have quantitative values as an integral component. Radiologic exams can be viewed, handled and interpreted differently. Other factors include illumination of the image, room lighting/darkening, eye fatigue and resolution of the interpreted image. An example of radiographic subjectivity is bone density evaluation. An image that would be interpreted as having normal bone density could be interpreted by another examiner as having low or high bone density. As long as cutoff points do not exist in such subjective evaluation methods, different opinions or estimations will persist. This fact can be clearly seen in the results of our study, considering the fact that our readers are experienced OMF radiologists, work at the same institution, and were calibrated prior to the start of the image interpretations. The results of our study suggest that reducing the spatial resolution of the image increases vulnerability to the radiographic evaluation subjectivity. This can be seen by looking at the differences between the values of the areas under the ROC curves of the two readers. The difference was highest in the 12-inch FOV when compared to the 6 and 9-inch FOVs. This means that an examiner of radiographic images can see margins of the IANC against the surrounding appearance of aligned parallel bony trabeculae. These margins in reality might not exist and another examiner will not see them. This could be due to the loss of image sharpness associated with lower resolution. This, in fact, can affect the accuracy of detectability of structures such as the mandibular canal on the image. In such cases when image resolution is reduced and subjectivity is increased it might be recommended to have the image reviewed by more than one clinician or OMF radiologist.

Clinicians looking for imaging of the mandibular canal should also take into consideration the radiation dose to the patient. A panoramic radiograph has a lower dose than both CBCT and CT (22, 36, 37) (Table XIII). Panoramic imaging is limited to 2 dimensions and this would make the desire for 3 dimensional images increase. Panoramic imaging is limited to the mesio-distal and supero-inferior dimensions. The bucco-lingual dimension or depth is missing in these images. Structures overlap in the bucco-lingual dimension and the exact position of the object might be difficult to localize. Both CBCT and medical CT are 3 dimensional imaging modalities with no superimposition of anatomic structures. Comparing CBCT with multislice CT as options for 3 dimensional imaging, CBCT has a significant advantage due to its considerably lower radiation dose (22). The CB MercuRay CBCT unit has different patient radiation doses depending on the size of the FOV and the mA setting. The smaller the FOV the lower the patient's dose will be (38) (Table XIII). This important advantage, coupled with the results of our study would suggest that the 6-inch FOV in the CB MercuRay CBCT unit is the best protocol for imaging the mandibular canal.

The 9 and 12-inch FOVs might be considered in cases where the mandibular canals and areas of the maxillary arch and sinuses are to be seen. An example is patients with multiple keratocystic odontogenic tumors (KOT) in the case of basal cell nevus syndrome. In these cases relation of the mandibular KOTs with the IANCs needs to be evaluated. On the other hand the determination of the extent of KOTs in the maxillary arch and sinuses might require wider scan area coverage. One larger FOV scan in this

example is better than exposing the patient to multiple smaller FOV scans that would expose the patient to more radiation. The larger FOVs also require careful interpretation of the images and consultation with an OMF radiologist or experienced clinician as suggested by the results of our study.

Imaging Modality	Effective dose (uSv)
Panoramic (OrthoPhos Plus DS)	13.3
Maxillo-mandibular CT scan	2100
Mercuray – 12-inch FOV 15–120 avg	1025.4
Mercuray – 9-inch FOV	435.5
Mercuray – 6-inch FOV (maxillary)	283.3
i-CAT – 12-inch FOV	193.4
i-CAT – 9-inch FOV	104.5
NewTom 3G – 12-inch FOV	58.9
NewTom 9000 – 9-inch FOV	51.7
Galileos default exposure	70
Galileos maximum exposure	128
J. Jorita Accuitomo (4 x 5 cm FOV)	5.0 - 20

Table XIII: Comparison of the effective doses of different imaging modalities used in the maxillofacial area including Panoramic (OrthoPhos Plus DS), medical CT and samples of CBCT units (CB Mercuray CBCT, i-CAT CBCT, NewTom 3G CBCT, NewTom 9000, Galileos and J. Morita Accuitomo). Table adapted from (22, 36, 37, 38) and Morita technical specifications

Conclusion

Important nerve innervation and blood supply to the mandibular teeth and surrounding structures, including the gingiva and lower lip, runs inside the IANC. When dental treatments, such as endodontic therapy, or surgical procedures, such as implant placement, exodontia or reduction of fractures are to be performed in the vicinity of the IANC, careful treatment planning is needed. This treatment planning should not be solely to treat the patient's signs and symptoms, but must be to avoid injury to the IANC.

Adequate imaging and detectability of the IANC can accomplish this. Our evaluation of the CB MercuRay CBCT unit that has 6-inch, 9-inch and 12-inch FOVs showed that CBCT is a good imaging modality for imaging of the IANC even though it is unable to detect clearly the IANC in all cases. The 6-inch FOV is the best imaging protocol on the CB MercuRay CBCT for imaging the IANC, with highest value of the area under the ROC curve when compared to the 9-inch and 12-inch protocols. The results of our study also suggest that the reduction in spatial resolution by increasing the size of the FOV makes detection of the IANC more vulnerable to subjectivity of the reader. The reduction of spatial resolution also leads to increased disagreements between readers during image interpretation. Even though the 9-inch and 12-inch FOV have lower values under their ROC curves, they can be used with caution; this means that careful examination of the image is advised in addition to consultation with an OMF radiologist or experienced clinician.

References

1. Shankland WE, 2nd. The position of the mental foramen in Asian Indians. *J Oral Implantol* 1994;20:118-123.
2. Sawyer DR, Kiely ML, Pyle MA. The frequency of accessory mental foramina in four ethnic groups. *Arch Oral Biol* 1998;43:417-420.
3. Bavitz JB, Harn SD, Hansen CA, Lang M. An anatomical study of mental neurovascular bundle-implant relationships. *Int J Oral Maxillofac Implants* 1993;8:563-567.
4. Fishel D, Buchner A, Hershkowitz A, Kaffe I. Roentgenologic study of the mental foramen. *Oral Surg Oral Med Oral Pathol* 1976;41:682-686.
5. Agthong S, Huanmanop T, Chentanez V. Anatomical variations of the supraorbital, infraorbital, and mental foramina related to gender and side. *J Oral Maxillofac Surg* 2005;63:800-804.
6. Neiva RF, Gapski R, Wang HL. Morphometric analysis of implant-related anatomy in Caucasian skulls. *J Periodontol* 2004;75:1061-1067.
7. Mraiwa N, Jacobs R, van Steenberghe D, Quirynen M. Clinical assessment and surgical implications of anatomic challenges in the anterior mandible. *Clin Implant Dent Relat Res* 2003;5:219-225.
8. Greenstein G, Tarnow D. The mental foramen and nerve: clinical and anatomical factors related to dental implant placement: a literature review. *J Periodontol* 2006;77:1933-1943.

9. Jerjes W, Upile T, Shah P, Nhembe F, Gudka D, Kafas P, McCarthy E, Abbas S, Patel S, Hamdoon Z, Abiola J, Vourvachis M, Kalkani M, Al-Khawalde M, Leeson R, Banu B, Rob J, El-Maaytah M, Hopper C. Risk factors associated with injury to the inferior alveolar and lingual nerves following third molar surgery-revisited. *Oral Surg Oral Med Oral Pathol Oral Radiol Endod* 2010;109:335-345.
10. Levine MH, Goddard AL, Dodson TB. Inferior alveolar nerve canal position: a clinical and radiographic study. *J Oral Maxillofac Surg* 2007;65:470-474.
11. Kovisto T, Ahmad M, Bowles WR. Proximity of the mandibular canal to the tooth apex. *J Endod* 2011;37:311-315.
12. Claeys V, Wackens G. Bifid mandibular canal: literature review and case report. *Dentomaxillofac Radiol* 2005;34:55-58.
13. Pogrel MA. Damage to the inferior alveolar nerve as the result of root canal therapy. *J Am Dent Assoc* 2007;138:65-69.
14. Escoda-Francoli J, Canalda-Sahli C, Soler A, Figueiredo R, Gay-Escoda C. Inferior alveolar nerve damage because of overextended endodontic material: a problem of sealer cement biocompatibility? *J Endod* 2007;33:1484-1489.
15. Valmaseda-Castellon E, Berini-Aytes L, Gay-Escoda C. Inferior alveolar nerve damage after lower third molar surgical extraction: a prospective study of 1117 surgical extractions. *Oral Surg Oral Med Oral Pathol Oral Radiol Endod* 2001;92:377-383.
16. Sisk AL, Hammer WB, Shelton DW, Joy ED, Jr. Complications following removal of impacted third molars: the role of the experience of the surgeon. *J Oral Maxillofac Surg* 1986;44:855-859.

17. Rood JP. Permanent damage to inferior alveolar and lingual nerves during the removal of impacted mandibular third molars. Comparison of two methods of bone removal. *Br Dent J* 1992;172:108-110.
18. Bruce RA, Frederickson GC, Small GS. Age of patients and morbidity associated with mandibular third molar surgery. *J Am Dent Assoc* 1980;101:240-245.
19. White SC. Cone-beam imaging in dentistry. *Health Phys* 2008;95:628-637.
20. Okano T, Harata Y, Sugihara Y, Sakaino R, Tsuchida R, Iwai K, Seki K, Araki K. Absorbed and effective doses from cone beam volumetric imaging for implant planning. *Dentomaxillofac Radiol* 2009;38:79-85.
21. Kositbowornchai S, Densiri-aksorn W, Piumthanaroj P. Ability of two radiographic methods to identify the closeness between the mandibular third molar root and the inferior alveolar canal: a pilot study. *Dentomaxillofac Radiol* 2010;39:79-84.
22. Ludlow JB, Ivanovic M. Comparative dosimetry of dental CBCT devices and 64-slice CT for oral and maxillofacial radiology. *Oral Surg Oral Med Oral Pathol Oral Radiol Endod* 2008;106:106-114.
23. Scarfe WC, Farman AG, Sukovic P. Clinical applications of cone-beam computed tomography in dental practice. *J can Dent Assoc* 2006;72:75-80.
24. Scarfe WC, Farman AG. What is cone-beam CT and how does it work? *Dent Clin North Am* 2008;52:707-30, v.
25. Baba R, Konno Y, Ueda K, Ikeda S. Comparison of flat-panel detector and image-intensifier detector for cone-beam CT. *Comput Med Imaging Graph* 2002;26:153-158.

26. Baba R, Ueda K, Okabe M. Using a flat-panel detector in high resolution cone beam CT for dental imaging. *Dentomaxillofac Radiol* 2004;33:285-290.
27. Sukovic P. Cone beam computed tomography in craniofacial imaging. *Orthod Craniofac Res* 2003;6 Suppl 1:31-6; discussion 179-82.
28. [Anonymous]. Use of cone-beam computed tomography in endodontics Joint Position Statement of the American Association of Endodontists and the American Academy of Oral and Maxillofacial Radiology. *Oral Surg Oral Med Oral Pathol Oral Radiol Endod* 2011;111:234-237.
29. Patel S, Dawood A, Ford TP, Whaites E. The potential applications of cone beam computed tomography in the management of endodontic problems. *Int Endod J* 2007;40:818-830.
30. Angelopoulos C, Thomas SL, Hechler S, Parissis N, Hlavacek M. Comparison between digital panoramic radiography and cone-beam computed tomography for the identification of the mandibular canal as part of presurgical dental implant assessment. *J Oral Maxillofac Surg* 2008;66:2130-2135.
31. Naitoh M, Nakahara K, Suenaga Y, Gotoh K, Kondo S, Arijji E. Comparison between cone-beam and multislice computed tomography depicting mandibular neurovascular canal structures. *Oral Surg Oral Med Oral Pathol Oral Radiol Endod* 2010;109:e25-31.
32. Feldkamp LA, Davis LC, Kress JW. Practical cone-beam algorithm. *J Opt Soc Am A* 1984; 1: 612–619.
33. Araki K, Maki K, Seki K, Sakamaki K, Harata Y, Sakaino R, Okano T, Seo K. Characteristics of a newly developed dentomaxillofacial X-ray cone beam CT scanner

(CB MercuRay): system configuration and physical properties. *Dentomaxillofac Radiol* 2004;33:51-59.

34. Landis JR, Koch GG. The measurement of observer agreement for categorical data. *Biometrics* 1977;33:159-174.

35. Xie Q, Wolf J, Tilvis R, Ainamo A. Resorption of mandibular canal wall in the edentulous aged population. *J Prosthet Dent* 1997;77:596-600.

36. Ngan DC, Kharbanda OP, Geenty JP, Darendeliler MA. Comparison of radiation levels from computed tomography and conventional dental radiographs. *Aust Orthod J* 2003;19:67-75.

37. Ludlow JB, Davies-Ludlow LE, Brooks SL. Dosimetry of two extraoral direct digital imaging devices: NewTom cone beam CT and Orthophos Plus DS panoramic unit. *Dentomaxillofac Radiol* 2003;32:229-234.

38. Ludlow JB, Davies-Ludlow LE, Brooks SL, Howerton WB. Dosimetry of 3 CBCT devices for oral and maxillofacial radiology: CB Mercuray, NewTom 3G and i-CAT. *Dentomaxillofac Radiol* 2006;35:219-226.